Published in IET Renewable Power Generation
Received on 7th October 2013
Revised on 10th February 2014
Accepted on 13th February 2014
doi: 10.1049/iet-rpg.2013.0324


ISSN 1752-1416

# Detection of rotor electrical asymmetry in wind turbine doubly-fed induction generators

*Mahmoud Zaggout[1,2], Peter Tavner[1], Christopher Crabtree[1], Li Ran[3]*

[1]*School of Engineering and Computing Sciences, Durham University, Durham, DH1 3LE, UK*
[2] *Department of Electrical Engineering, Faculty of Engineering, Misurata University, Misurata, Libya*
[3]*School of Engineering, University of Warwick, Coventry, CV4 7AL, UK*
*E-mail: m.n.zaggout@durham.ac.uk*

**Abstract:** This study presents a new technique for detecting rotor electrical faults in wind turbine doubly-fed induction generators (DFIGs), controlled by a stator field-oriented vector control scheme. This is a novel method aimed at detecting and identifying rotor electrical asymmetry faults from within the rotor-side inverter control loop, using the error signal, to provide a future method of generator condition monitoring with enhanced detection sensitivity. Simulation and experimental measurements of the proposed signals were carried out under steady-state operation for both healthy and faulty generator conditions. Stator current and power were also investigated for rotor electrical asymmetry detection and comparison made with rotor-side inverter control signals. An investigation was then performed to define the sensitivity of the proposed monitoring signals to fault severity changes and a comparison made with previous current, power and vibration signal methods. The results confirm that a simple spectrum analysis of the proposed control loop signals gives effective and sensitive DFIG rotor electrical asymmetry detection.

## 1 Introduction

Over the last 15 years, variable speed wind turbines (WTs) with doubly-fed induction generators (DFIGs) have become the most applied WT technology and the drive train choice for up to 60% of large, >1.5 MW WTs [1]. The typical configuration of these WTs consist of a wound rotor induction generator (WRIG) with stator winding connected directly to the grid, whereas the rotor winding is connected via slip-rings to a partially rated back-to-back converter and operating as a DFIG, as shown in Fig. 1*a*. In this system, the variable speed range is approximately ±25% of the synchronous speed, as shown in Fig. 1*b*. The rating of the power electronic converter is only 30% of the generator capacity, which makes this concept attractive and popular from an economic point of view.

From Fig. 1*b*, whenever the wind speed is below the rated the WT-DFIG operates at variable speed, under the control of the converter. However, when the wind speed reaches the rated, the WT-DFIG delivers full power, fixed at the top of its speed range, subject to variations because of wind turbulence.

Like every electrical machine, these generators are prone to electromechanical faults and require attention at the incipient fault stage to avoid fault escalation leading to breakdown. However, a survey to compare the failure rates of WT induction generator (IG) with other machines in industrial applications based on data reported in [2–7] has shown the significance of WT generator failures, which are mainly concentrated in the rotor, stator and machine bearings, as shown in Fig. 2.

The study also showed that the failures associated with the rotor and other parts contribute significantly to the total number of induction machine failures, particularly in wind applications, ranging from 12 to 50% of generators failures. Owing to these percentages, WT-IG rotor fault diagnosis has received considerable attention and WT DFIG rotor asymmetry has been shown to be a significant indicator of WT generator faults, caused by either rotor winding or brush-gear defects. Previous work investigated the effects of induction machine rotor faults on the machine electrical signals [8–9] or mechanical signals [10]. Each method has its advantages but it is essential that the selected method should have a high sensitivity to incipient faults and prevent unexpected breakdown or total destruction of the machine.

Nowadays, in most applications the induction machine is part of a complex system with closed-loop control. In this case, condition monitoring techniques usually applied to line-fed, open-loop machines may be ineffective, as the control modifies the behaviour of machine signals and masks their information. Therefore other signal behaviours should be investigated and more sophisticated procedures adopted to find better indices to assess machine condition. Consequently a number of authors have investigated fault detection in closed-loop induction machines using machine control loop signals. Based on simulation and experimental investigation, frequency analyses of control current signals have been presented in [11] to diagnose the stator and rotor faults of controlled squirrel cage induction motors (SCIMs). A new online method based on measured torque control

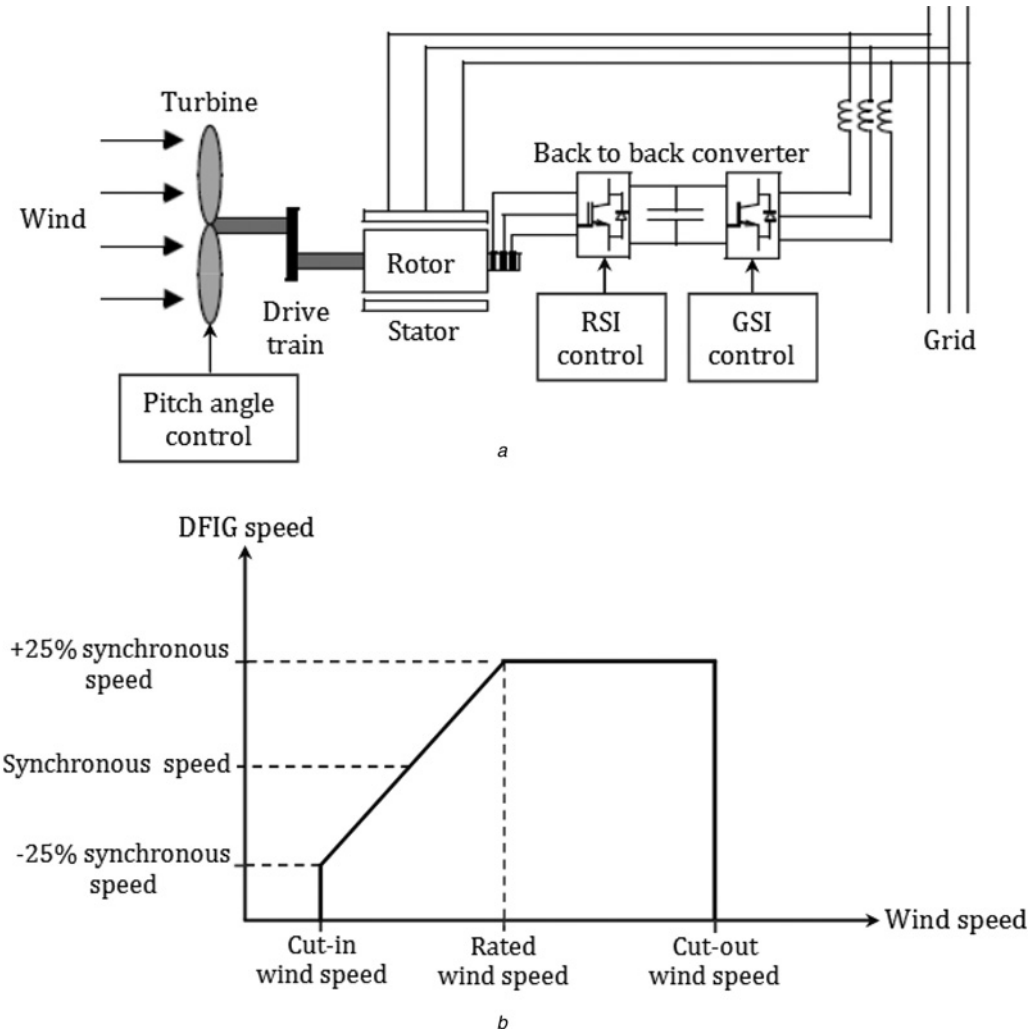


**Fig. 1** *Typical configuration of WTs.*

*a* Variable speed WT with DFIG controlled with a partial-scale power converter
*b* Generator speed against wind speed

current component and calculated slip frequency was proposed in [12]. Later, diagnosis of SCIM rotor faults through current controller error signals, current controller output signals and the estimated rotor flux analyses were studied in [13]. Another investigation of rotor faults in different controller topologies, particularly in IM open or closed speed loop control, was presented in [14]. More recently, this research was developed [15] to include a SCIM with direct torque control.

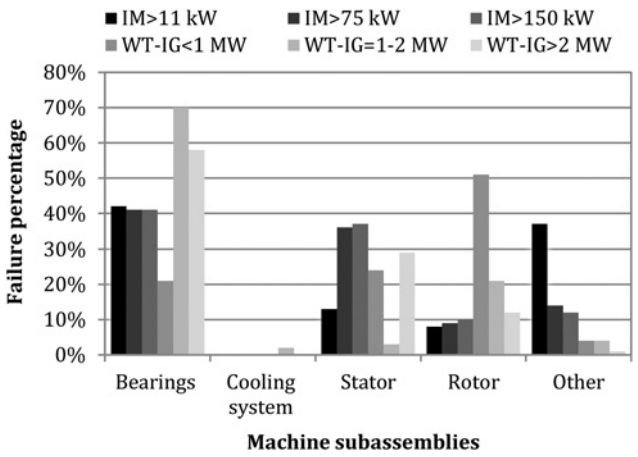


**Fig. 2** *Distribution of failed subassemblies in induction machines based on data reported in [2–7]*

However, understanding the influence of WT-IG failures on different generator control variables and using these signals for monitoring the WT-IGs has received little research attention. A simulation and experimental study was presented in [16] to identify the best diagnostic procedure for unbalanced DFIG phase fault detection. It was confirmed that the current signature analysis technique could be utilised, but a more interesting technique would be to use rotor modulation signal spectral analysis. More recently, the sensitivity of rotor modulation signal spectra, with respect to the variation of current loop bandwidth, was evaluated in [17] as a new and reliable diagnostic index.

The work described in this paper extends previous WT-IG failure diagnosis research in [8], based on stator current and total power spectra, to consider WT-DFIG fault detection using generator control loop signals. It particularly concentrates on the rotor side inverter (RSI) and compares the effectiveness of control loop fault detection signals with stator current, total power and vibration signals. Frequency analysis of the RSI current control error signal is proposed as an effective new diagnostic index for




doi: 10.1049/iet-rpg.2013.0324

WT-DFIGs. Using such signals will improve WT condition monitoring because:

- Control error signals are dominated by the fault effect and their spectra clearly show faulty harmonics allowing them to be detected more clearly, compared to generator signal spectra.
- These signals are already available for control purposes and can easily be measured, giving them an advantage over some conventional techniques, which require costly additional instrumentation and data processing.

The novelty of the paper is its consideration of control signals for condition monitoring of a variable speed WT-DFIG, demonstrated by simulation and verified on a realistic Test Rig. The rest of the paper is organised as follows: Section 2 gives an in-depth investigation of the influence of rotor electrical asymmetry on RSI control signals. Section 3 describes the overall simulation and experimental tools. Section 4 presents the RSI control scheme. Section 5 describes the simulation results for the proposed signals, and then confirmed by experimental results. The improvement in condition monitoring detection performance with the proposed method has been demonstrated in comparison with previous stator current, power and vibration analysis methods. These comparisons will demonstrate that the proposed method can reliably detect rotor fault, regardless of fault severity.

## 2 Rotor electrical asymmetry

Generator rotor faults, because of the increasing resistance or open-circuit of one or more of the rotor windings or brush-gear circuits, results in rotor electrical asymmetry. Such faults are caused by a combination of magnetic, thermal and mechanical stresses acting on the rotor, varying dynamically with loading and environmental conditions. Although rotor asymmetries do not initially cause a machine to fail, they can have serious secondary effects, increasing losses, reducing efficiency and lowering generator and turbine reliability. However all of this could be avoided if the machine was supervised by an appropriate condition monitoring system.

### 2.1 Basic derivation of electrical frequencies

The sequence of electromagnetic and mechanical phenomena due to asymmetry in the stator or rotor of an induction machine was explained in [18]. They give rise to a series of harmonic components in the rotor current at frequencies $-sf, \pm 3sf, \ldots, \pm isf$, where $s$ is the generator slip, $f$ is the stator frequency and $i = 1, 3, 5, \ldots$ Although the RSI controller is designed and implemented for a healthy generator, its closed-loop action attempts to ensure a correct operation even in the presence of any rotor asymmetry. In this case, the PI current control loops try to impose balanced rotor current references by applying unbalanced voltages to the rotor winding. Therefore typical generator current faulty harmonics might become less visible because of the compensating action of the RSI controller. In contrast, these fault-components should remain clearly observable in the error signals inside rotor current PI controller, allowing these signals to be considered as new effective diagnostic indices.

The rotor faulty harmonics ($\pm isf$) will be transferred into RSI control loop signals and are expected to produce a relevant harmonic in the $d$- and $q$-rotor currents ($i_{dr}$ and $i_{qr}$) at $\pm 2msf$ where $m = 1, 2, 3, \ldots$ Under rotor fault condition, the $d$- and $q$-rotor currents, in the stator flux linkage reference frame, can be written as

$$i_{dr}(t) = I_{dr_0}(t) + \sum_{m=1}^{\infty} I_{dr_{\pm 2m}} \cos(2\pi(\pm 2m\text{sf})t + \varnothing_{dr_{\pm 2m}}) \quad (1)$$

$$i_{qr}(t) = I_{qr_0}(t) + \sum_{m=1}^{\infty} I_{qr_{\pm 2m}} \cos(2\pi(\pm 2m\text{sf})t + \varnothing_{qr_{\pm 2m}}) \quad (2)$$

where $I_{dr}$ and $I_{qr}$ are the harmonic magnitudes of $d$- and $q$-rotor currents, $\varnothing_{dr}$ and $\varnothing_{qr}$ are the harmonic phase shifts of $d$- and $q$-rotor currents. Subtracting (1) from the $d$-rotor reference current ($i_{dr\ ref}$) and (2) from the $q$-rotor reference current ($i_{qr\ ref}$), the error signals ($\varepsilon i_{dr}$ and $\varepsilon i_{qr}$) inside PI control loops is obtained. Theoretically $i_{dr\ ref}(t) \cong I_{dr_0}(t)$ and $i_{qr\ ref}(t) \cong I_{qr_0}(t)$. Then, the error signals can be written as

$$\varepsilon i_{dr}(t) \cong -\sum_{m=1}^{\infty} I_{dr_{\pm 2m}} \cos(2\pi(\pm 2m\text{sf})t + \varnothing_{dr_{\pm 2m}}) \quad (3)$$

$$\varepsilon i_{qr}(t) \cong -\sum_{m=1}^{\infty} I_{qr_{\pm 2m}} \cos(2\pi(\pm 2m\text{sf})t + \varnothing_{qr_{\pm 2m}}) \quad (4)$$

From (3) and (4), as mentioned before, the current error signals are expected to contain mainly the faulty harmonics, which will dominate the error signal spectrum and can be detected by applying a simple FFT algorithm. In this work, the used FFT algorithm analyse the component signals in both the positive and negative sequence, plotting both on the positive axis of the spectrum. Therefore attention will be focused only on the $2sf$ component inside the control signals, as well as the $(1-2s)f$ in the total power and stator current, respectively.

### 2.2 Fault representation

In order to test several fault situations in a machine operating as IG in a WT system, the main problem is to realise a fault situation similar to reality. In practice, rotor electrical asymmetries can be modelled by inserting an additional resistance in series with the rotor phase windings. In this research, the rotor asymmetry was created on an experimental Test Rig, by means of external variable resistor ($R_{ex}$) connected into one phase of the rotor circuit via the machine slip rings. This allows different asymmetry levels to be introduced in a controlled fashion. When $R_{ex}$ is greater than zero the faulted phase resistance is present. For clarity, the asymmetric rotor resistance is given as a percentage of the balanced phase resistance, where rotor asymmetry, $\Delta R$, in percent, is

$$\Delta R(\%) = \frac{R_{ex}}{R_r} \times 100 \quad (5)$$

where $R_r$ is the healthy rotor phase resistance. The values of $R_{ex}$ and $\Delta R$ depend on the unbalance severity. Note that rotor unbalance can be in one phase or more and it will produce the same relative frequency harmonics in the machine or control signals. In the same way, the fault can be applied to a MATLAB model of the Test Rig.

## 3 Investigation tools

The proposed technique in this paper has been validated experimentally on a Durham Test Rig which was designed to investigate and monitor various WT drive-train failure modes. Over the last few years, this Rig has been used to develop a number of WT generator condition monitoring algorithms [8, 19, 20]. Fig. 3 shows the block diagram of the Test Rig developed to operate as a WT-driven DFIG. It comprises a 4-pole, 30 kW WRIG driven through a 5:1 gearbox by a 54 kW DC motor, which simulates the WT. The stator windings of the WRIG were directly connected to the grid whereas the rotor windings were fed from a PWM-RSI controlled by an xPC TargetBox real-time system. The DC Link was provided by a battery, to avoid any interaction from the GSI. Therefore the machine operates as a DFIG, whose details are given in the Appendix. The RSI control algorithm is designed based on a stator field-oriented vector control scheme. The controller model was represented initially in the MATLAB Simulink and when the operator is ready to run the controller, the model can be simply compiled to be executable and loaded onto the xPC TargetBox. However, because of the limitations of the xPC TargetBox hardware in synchronising the generated phase PWM signals both the DC-link voltage and the stator voltage were purposely reduced, compared to the generator and converter rating, to provide lower distortion control and generator signals and increase safety. This voltage reduction lowered the machine flux density. This was not expected to affect the prospective accuracy of a proposed rotor asymmetry detection technique on a WT-DFIG operating at normal operating voltage and flux density, when the PWM signals are perfectly synchronised. The Test Rig was used to obtain the measured results presented in this paper.

A mathematical model of the experimental Test Rig was built in MATLAB Simulink by the authors to represent all the mechanical and electrical parts of the Rig, as well as the grid and losses. The validity of the experimental results, in time and frequency domains, was verified by comparison with this model, which was used to obtain all the simulated results presented in this paper.

## 4 Rotor-side inverter controller

Similar to a real WT-DFIG, the rotor is associated with a back-to-back converter and the stator directly connected to the grid in the closed-loop Test Rig configuration. The RSI is controlled in a synchronously rotating $dq$-axis frame, with the $d$-axis oriented along the stator flux vector position and the $q$-axis leading the $d$-axis by 90°. In this way, a decoupling between the electrical torque and the rotor excitation current is obtained in order to control stator active power. The stator currents are assumed to be positive when flowing from the grid into the machine. Since the stator is connected to the grid, and the influence of the stator resistance is small, the stator magnetising current can be considered constant. Under stator-flux orientation, the active and reactive powers ($P_s$ and $Q_s$) delivered by the stator of the machine can be written as a function of $dq$-rotor current components and stator voltage magnitude ($|V_s|$) as [1]

$$P_s \cong -1.5\frac{L_M}{n_{sr}L_s}|V_s|i_{qr} \tag{6}$$

$$Q_s \cong 1.5\frac{L_m}{L_s}|V_s|\left(\frac{|V_s|}{\omega L_m}-\frac{i_{dr}}{n_{sr}}\right) \tag{7}$$

where $L_m$ and $L_s$ are the generator magnetising and stator self-inductances, $n_{sr}$ is the stator–rotor turns ratio and $\omega$ is the stator flux speed. By assuming the stator voltage magnitude and frequency are constant, the stator active power can be considered proportional to the $q$-axis rotor current component and the stator reactive power related to the $d$-axis rotor current component.

## 5 Results

In order to verify the proposed detection method several tests were carried out on the physical Test Rig and its MATLAB Simulink model under both healthy and faulty conditions. The analysis was achieved by comparing the harmonic spectra of stator current and power with those of $d$- and

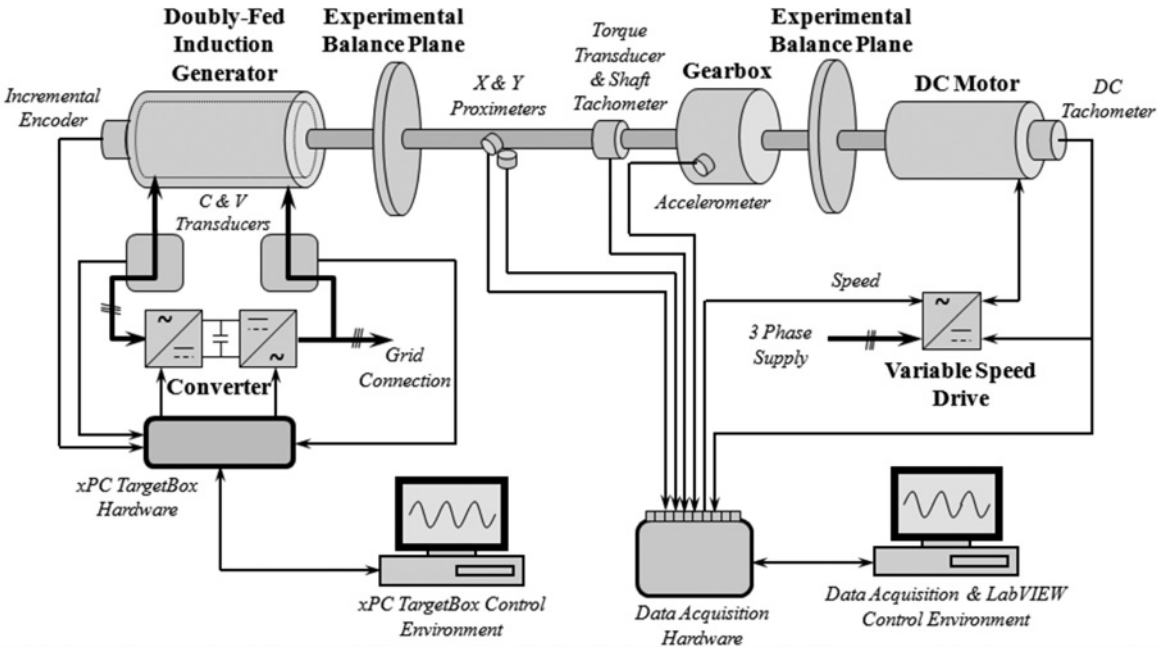


**Fig. 3** *Schematic diagrams of the WT drive train Test Rig with DIFG*




doi: 10.1049/iet-rpg.2013.0324

$q$-rotor current error signals. The harmonic spectra were obtained by applying an FFT algorithm to instantaneous values of the monitored variables which were sampled at 5 kHz.

### 5.1 Fixed speed operation

In both the simulation and experimental environments, the system was run at super-synchronous fixed speed of 1600rev/min, with the generator delivering 4.7 kW and absorbing 1.95 kVAr, under healthy or faulty conditions. This speed Test Rig operation was undertaken with the speed of the Test Rig DC drive motor controlled by a turbine model, developed, tested and verified by Strathclyde University, representing a WT operating above rated wind speed at its rated power, as shown in Fig. 1*b*. The speed of the Test Rig was approximately constant, but varied because of turbulence of the wind driving the turbine model and the action of the DFIG RSI control loop to maintain speed constant. The effect of any rotor electrical asymmetry on the WT generator speed would have been negligible, as the turbine and generator inertia damp this effect. The healthy rotor resistance, including internal winding resistance, was 0.235 Ω per phase and additional resistance up to 0.047 Ω was successively added to one phase to give 20% unbalance. To simplify the presentation of results, all signal spectral analyses have been normalised to 0 dB at the highest harmonic component magnitude, depending on the signal type.

*5.1.1 Simulated results:* Simulations were carried out operating the machine in a noise-free environment. For balanced and unbalanced operations, the $dq$-rotor error current spectra are presented in Fig. 4. The healthy current spectra, Figs. 4*a* and *c*, indicate the fundamental harmonic at 0 Hz, 0 dB and a set of harmonics at 19.5, 39, 58.5, 78 and 97.5 Hz, produced by the PWM process used in the RSI. This set of harmonics is less visible in the faulty spectra shown in Figs. 4*b* and *d*. The faulty spectra show a significant rise in the magnitude of the 2$sf$ component at frequency at 6.5 Hz, as expected, which dominate the whole two spectra.

Simulated healthy and faulty stator current and total power spectra for this condition are shown in Fig. 5. Only one phase current signal is presented and analysed here, as is usually the case for Motor Current Signal Analysis (MCSA). The healthy current spectrum in Fig. 5*a* indicates the fundamental harmonic at 50 Hz whereas the power spectrum in Fig. 5*c* indicates the fundamental harmonic at 0 Hz. They show that the reflection of rotor switching harmonics is not visible in the stator current compared to the total power. The faulty stator current and total power spectra in Figs. 5*b* and *d* show visible harmonics related to the fault at 56.5 Hz and 6.5 Hz with magnitudes of −66 dB and −71 dB. Note that, both the total power and stator current faulty harmonics are not as large in magnitude as in the case of error signals, Fig. 4.

It can be observed that the harmonic spectra of the $d$- and $q$-rotor current error signals show larger amplitude harmonic components than at other fault-related frequencies, giving a better fault indication. Thus, the proposed method is interesting and could be adopted for improved condition monitoring.

*5.1.2 Measured results:* For comparison with simulated results, in the physical Test Rig the RSI controller and DFIG measured signals were collected, with rotor circuits balanced or unbalanced, from the xPC TargetBox. However, the measured signals now incorporate higher levels of noise than the simulated signals. This noise was caused experimentally by

- The small but continuous grid frequency fluctuation, between 49.9 and 50.1 Hz;
- DFIG stator magnetising unbalance;
- University site grid voltage unbalance which, although small, contributes to stator unbalance and noise.

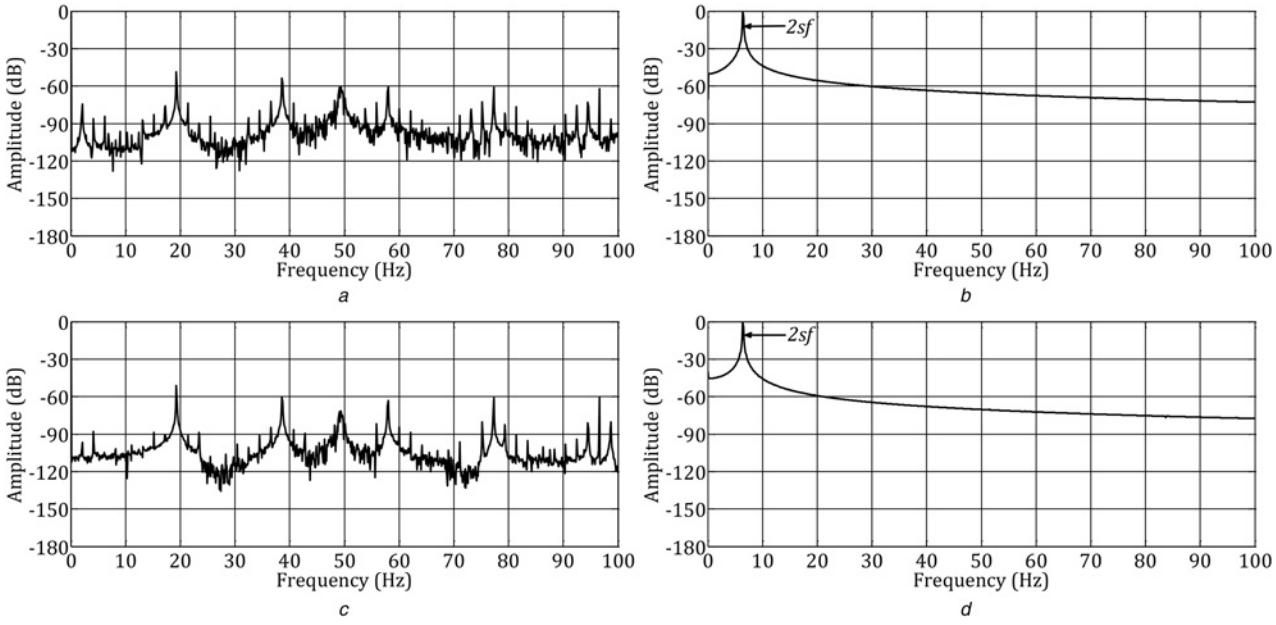


**Fig. 4** *Healthy and faulty simulated spectra for generator control signals*

*a* d-rotor current error-healthy condition
*b* d-rotor current error-faulty condition
*c* q-rotor current error-healthy condition
*d* q-rotor current error-faulty condition

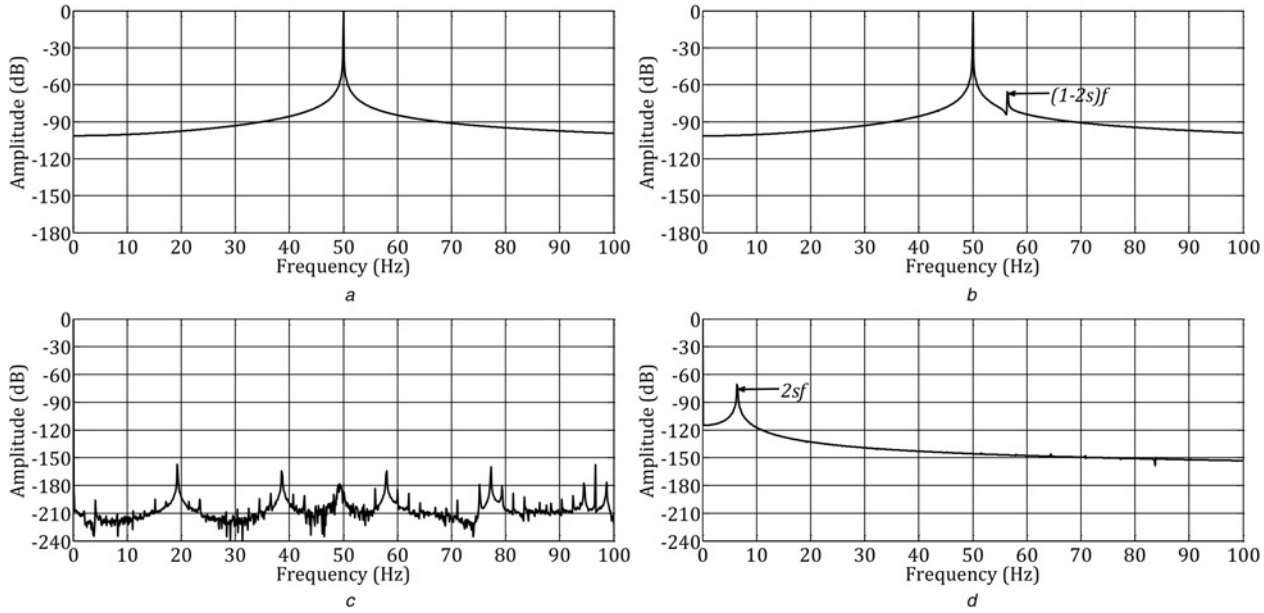


**Fig. 5** *Healthy and faulty simulated spectra for stator current and total power signals*

*a* Stator current-healthy condition
*b* Stator current-faulty condition
*c* Stator total power-healthy condition
*d* Stator total power-faulty condition

These noise sources were unavoidable in the current measurements from the physical Test Rig; however, they are not specific only to the Test Rig but would also be present in a real WT-DFIG, so any functioning condition monitoring system needs to accommodate them.

Frequency analysis of the error signals is shown in Fig. 6. From these figures, the harmonic $2sf$ related to the fault presence is located at 6.5 Hz with a magnitude of −28 and −22 dB for *d*-and *q*-rotor error current spectra, respectively. However, comparing with the simulation results in Fig. 4, it can be seen that these magnitudes are not the highest values in this case and the highest magnitudes appear at 100 Hz in both spectra. These harmonics, as explained above, are related to the stator fault contributed by a little grid voltage unbalance.

The stator current harmonic spectra are presented in Figs. 7*a* and *b*. The magnitude of the faulty harmonic is less visible with a value of −47 dB for the stator current at

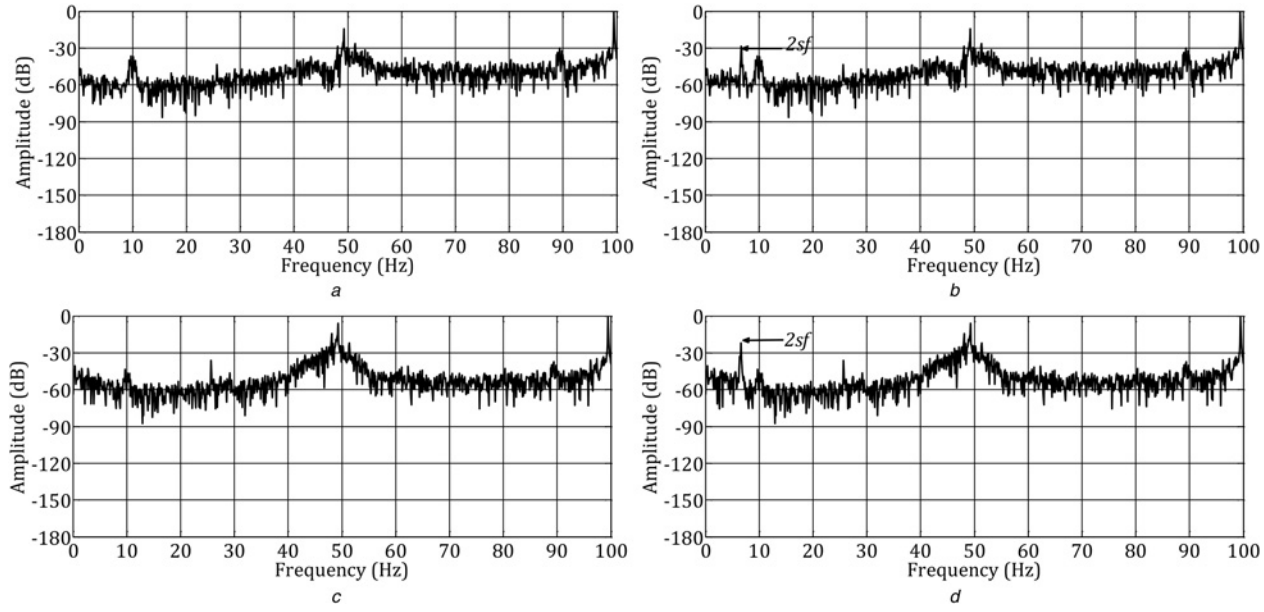


**Fig. 6** *Healthy and faulty measured spectra for generator control signals*

*a* d-rotor current error-healthy condition
*b* d-rotor current error-faulty condition
*c* q-rotor current error-healthy condition
*d* q-rotor current error-faulty condition




doi: 10.1049/iet-rpg.2013.0324

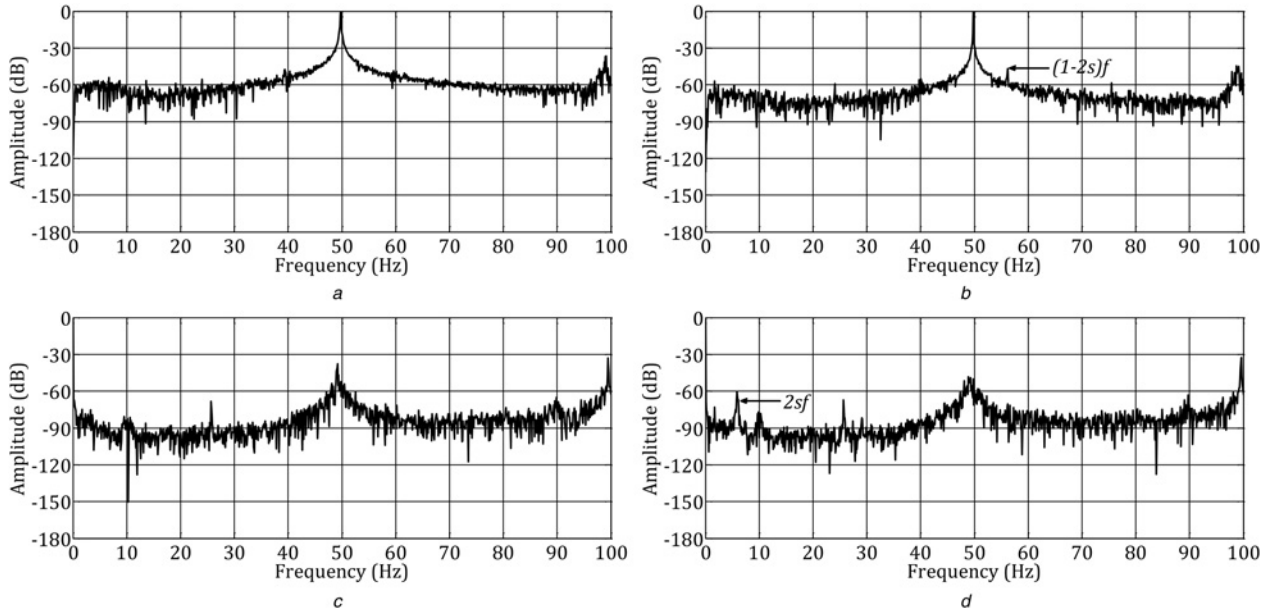


**Fig. 7** *Healthy and faulty measured spectra for stator current and total power signals*

*a* Stator current-healthy condition
*b* Stator current-faulty condition
*c* Stator total power-healthy condition
*d* Stator total power-faulty condition

56.5 Hz (1–2s)*f*. The total power harmonic spectra are presented in Figs. 7*c* and *d* and the faulty harmonic component magnitude at 6.5 Hz (2*sf*) is −60 dB.

Again, these experimental results confirm that the control error signals have faulty component magnitudes at frequency (2*sf*) much higher than the other signals used in this research. This shows that the proposed technique has the potential to detect an incipient electrical asymmetry fault on a WT-DFIG, since the magnitude of the characteristic harmonic frequency can be easily detected.

### 5.2 Signal sensitivity on faulty detection

From the simulation and experimental results, it can be observed that all signal frequency analyses show an increase in the power level of the fault-frequency components. However, the signal that provides the best fault detection depends not only on the faulty harmonic magnitude but also on its sensitivity. The higher the sensitivity, the better the fault signature resolution. To verify the sensitivity achievable using the control and other signals as diagnostic indices, further simulation and experimental tests were carried out with the Test Rig DFIG in a 1400 rev/min steady-state condition at various fault-severities. The sensitivity values are obtained from the simulated and measured results by

$$\text{Sensitivity(dB)} = 10\log_{10}\left(\frac{A_\text{f} - A_\text{h}}{A_\text{h}}\right) \tag{8}$$

where $A_\text{f}$ and $A_\text{h}$ are the magnitudes of the faulty and healthy harmonic components. Complete results of the sensitivity for

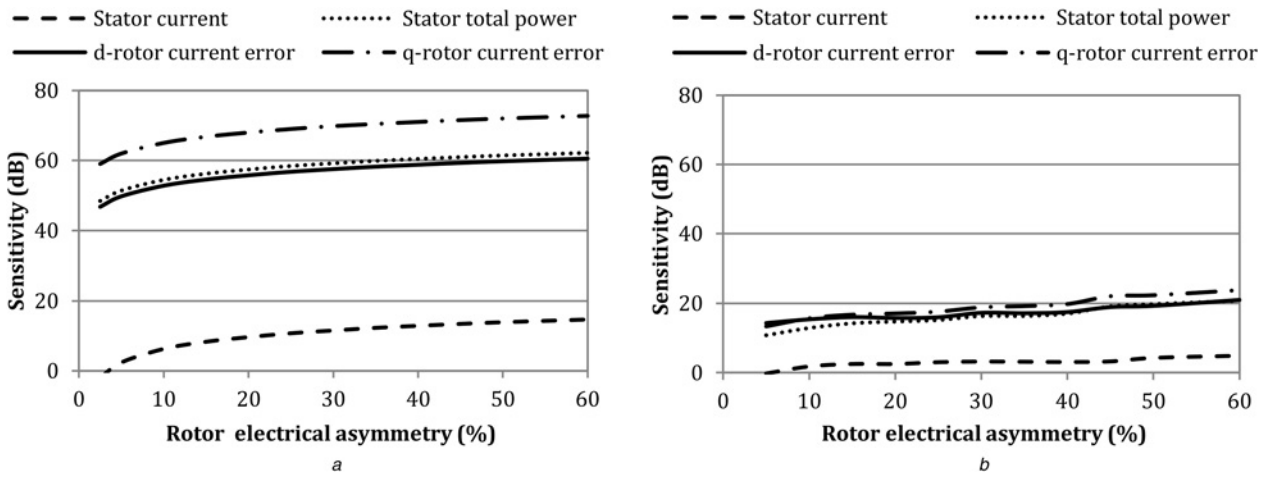


**Fig. 8** *Sensitivity from*

*a* Simulation data
*b* Measured Test Rig data

**Table 1** Comparison of fault detection sensitivities between open- and closed-loop Test Rig

| Test Rig system | Closed-loop system | | Open-loop system | | | | |
|---|---|---|---|---|---|---|---|
| signal type | current error signals inside RSI | | stator current | | stator total power | | vibration |
| | $\varepsilon i_{dr}$ | $\varepsilon i_{qr}$ | | | | | |
| frequency analysis | FFT | | frequency tracking algorithm | | | | SBPF |
| fault type | 20% rotor electrical asymmetry | | 23% rotor electrical asymmetry | | | | missing tooth of high speed shaft pinion |
| harmonics of interests | $2sf$ | | $(1-2s)f$ | $(3-2s)f$ | $2sf$ | $(2-2s)f$ | $2f_{mesh,HS}$ and its first five sideband peaks on each side |
| stator voltage | 78 V | | | | | 230 V | |
| sensitivity calculated at 1550 rev/min | 14.3 dB | 15.2 dB | 3.0 dB | 4.7 dB | 6.7 dB | 4.9 dB | 5.1 dB |
| sensitivity calculated at 1600 rev/min | 14.6 dB | 15.3 dB | 3.7 dB | 6.9 dB | 7.3 dB | 6.0 dB | 4.6 dB |

the four signal types are summarised and compared in Fig. 8. It can be seen that the sensitivity of all signals, both simulated and measured, increased with fault severity. From Fig. 8*a*, the sensitivities of the simulated control error signals had high values with the ability to detect even small fault severities. However, the *q*-rotor current error sensitivity was higher than the *d*-rotor current error sensitivity as well as those of the stator

The measured results, Fig. 8*b*, again show that despite the experimental effects of noise the *q*-rotor current error signal still has higher sensitivity over the other signals. They show a decreased sensitivity compared with simulation results, because of the noise in the measured signals, however, the results still show a significant and usable sensitivity for condition monitoring purposes.

From these results, it is evident that control signals, *d*- and *q*-rotor current errors, are sensitive to any rotor electrical asymmetry, with an advantage to the *q*-rotor current error compared to *d*-rotor current error, stator power or current.

Further tests have also been carried out with the Test Rig operating as when the WT was operating below rated wind speed and therefore rated power, see Fig. 1*b*, operating under full variable speed conditions. The results are similar to those presented here but have been omitted from this paper because of limitations of space.

### 5.3 Test Rig open and closed-loop fault detection sensitivities

As mentioned in Section 3, the open-loop Test Rig has been used in previous work to develop other techniques for WT-IG fault detection. One of these techniques is the frequency tracking algorithm based on stator line current and total power analysis [8], which investigated rotor electrical asymmetry detection for faults similar in magnitude to this paper. More recently, another technique was introduced in [21] based on the sideband power factor (SBPF) algorithm for WT gearbox fault detection by vibration analysis. The SBPF was successful in detecting gearbox tooth faults on a high speed shaft pinion. New work is being done to extend the vibration analysis for rotor electrical asymmetry detection in WRIG but results are not yet available. Therefore only the vibration analysis results for gearbox fault detection are presented in this comparison. Table 1 shows an experimental comparison between fault detection sensitivities on the closed-loop Test Rig using RSI control signals and open-loop Test Rig using stator current, power and vibration signals.

As can be seen from Table 1, the RSI control current error fault sensitivity is much higher than the frequency tracking algorithm with the same fault magnitude. This comparison confirms that the closed-loop detection sensitivities, even in the presence of noise, are considerably greater than they were achieved open loop with current, and power signals. This is because, as shown in (3) and (4), the *d*- and *q*-current error signals in the closed-loop system are mainly the reflection of rotor health condition changes whereas in the open-loop system the fault-related response is influenced by more factors than the fault. A direct comparison with the SPBF vibration results for electrical fault detection will be possible once more results are available.

## 6 Conclusions

This paper has demonstrated a new WT-DFIG rotor fault detection technique based on frequency analysis of the *d*- and *q*-rotor error current signals inside the DFIG RSI controller loop.

- The development of fault harmonics inside the proposed signal spectra has been explained.
- An RSI stator flux-oriented vector control scheme has been set up to verify this technique.
- A set of simulated and measured results have been obtained from a physical Test Rig and its validated model under fixed speed operating conditions, representing the conditions when the WT would be at full power.
- It has been shown that *d*- and *q*-rotor current error signals have characteristic frequencies that are a strong diagnostic index for rotor electrical asymmetry.
- The study has also clearly shown that the proposed *q*-control error signal provides better sensitivity to faults than stator current or total power signals and is a successful diagnostic even for small faults.
- Fault detection sensitivity in the closed-loop WT-DFIG Test Rig from the RSI control signals has a better sensitivity than previously published fault detection on an the open-loop WT-IG Test Rig from vibration, current and power signals.
- This technique is simple, attractive and could easily be extended to diagnose other generator or embedded turbine faults.
- Because of limitations of space in this paper, investigation of the method under full variable speed conditions, when the WT is below rated power, will be reported in a later publication.




doi: 10.1049/iet-rpg.2013.0324

• This study has shown that the measured results gave a lower sensitivity to faults than simulated results because of noise in the experimental system, which requires future investigation.

## 7 Acknowledgments

This work was supported by the UK EPSRC as part of the Supergen Wind Consortium under grant EP/D034566/1 and the Libyan Government by a PhD scholarship for the first author. The authors would like to thank the National Renewable Energy Centre, Blyth, for their assistance in the original provision of the Test Rig.

## 8 References

1 Zaggout, M.: 'Wind turbine generator condition monitoring via the generator control loop', *PhD thesis, School of Engineering and Computing Sciences*, Durham University, 2013
2 Motor Reliability Working Group: 'Report of large motor reliability survey of industrial and commercial installations, Part I', *IEEE Trans. Ind. Appl.*, 1985, **IA-21**, (4), pp. 853–864
3 Motor Reliability Working Group: 'Report of large motor reliability survey of industrial and commercial installations, Part II', *IEEE Trans. Ind. Appl.*, 1985, **IA-21**, (4), pp. 865–872
4 Motor Reliability Working Group: 'Report of large motor reliability survey of industrial and commercial installations, Part III', *IEEE Trans. Ind. Appl.*, 1987, **IA-23**, (1), pp. 153–158
5 Albrecht, P., Appiarius, J., McCoy, R., Owen, E., Sharma, D.: 'Assessment of the reliability of motors in utility applications-updated', *IEEE Trans. Energy Convers.*, 1986, **EC-1**, (1), pp. 39–46
6 Thorsen, O., Dalva, M.: 'A survey of faults on induction motors in offshore oil industry, petrochemical industry, gas terminals, and oil refineries', *IEEE Trans. Ind. Appl.*, 1995, **31**, (5), pp. 1186–1196
7 Alewine, K., Chen, W.: 'Wind turbine generator failure modes analysis and occurrence'. NREL, Lecture notes, September 2011
8 Djurovic, S., Crabtree, C., Tavner, P., Smith, A.: 'Condition monitoring of wind turbine induction generators with rotor electrical asymmetry', *IET Renew. Power Gener.*, 2012, **6**, (4), pp. 207–216
9 Ceban, A., Pusca, R., Romary, R.: 'Study of rotor faults in induction motors using external magnetic field analysis', *IEEE Trans. Ind. Electron.*, 2012, **59**, pp. 2082–2093
10 Li, W., Mechefske, C.: 'Detection of induction motor faults: A comparison of stator current, vibration and acoustic methods', *J. Vib. Control*, 2006, **12**, (2), pp. 165–188
11 Bellini, A., Filippetti, F., Franceschini, G., Tassoni, C.: 'Closed-loop control impact on the diagnosis of induction motors faults', *IEEE Trans. Ind. Appl.*, 2000, **36**, (5), pp. 1318–1329
12 Serna, E., Pacas, J.: 'Detection of rotor faults in field oriented controlled induction machines'. Proc. IEEE Industrial Applications Conf. 41st IAS Annual Meeting, Tampa, FL, 2006, pp. 2326–2332
13 Cruz, S., Cardoso, A.: 'Fault indicators for the diagnosis of rotor faults in FOC induction motor drives'. Proc. IEMDC, Antalya, May 2007, vol. 2, pp. 1136–1141
14 Concari, C., Franceschini, G., Lorenzani, E., Tassoni, C., Toscani, A.: 'Severity assessment of rotor faults in closed loop induction drives by different approaches'. Proc. SDEMPED, Cracow, 2007, pp. 309–315
15 Concari, C., Franceschini, G., Tassoni, C.: 'Rotor fault detection in closed loop induction motors drives by electric signal analysis'. Proc. ICEM, Vilamoura, 2008
16 Stefani, A., Yazidi, A., Rossi, C., Filippetti, F., Casadei, D., Capolino, G.: 'Doubly fed induction machines diagnosis based on signature analysis of rotor modulating signals', *IEEE Trans. Ind. Appl.*, 2008, **44**, (6), pp. 1711–1721
17 Casadei, D., Filippetti, F., Rossi, C., Stefani, A.: 'Closed loop bandwidth impact on doubly fed induction machine asymmetries detection based on rotor voltage signature analysis'. Proc. 43rd UPEC, Padova, 2008, pp. 1–5
18 Filippetti, F., Franceschini, G., Tassoni, C., Vas, P.: 'AI techniques in induction machines diagnosis including the speed ripple effect', *IEEE Trans. Ind. Appl.*, 1998, **34**, (1), pp. 98–108
19 Watson, S., Xiang, B., Yang, W., Tavner, P., Crabtree, C.: 'Condition monitoring of the power output of wind turbine generators using wavelets', *IEEE Trans. Energy Convers.*, 2010, **25**, pp. 715–721
20 Yang, W., Tavner, P., Wilkinson, M.: 'Condition monitoring and fault diagnosis of a wind turbine synchronous generator drive train', *IET Renew. Power Gener.*, 2009, **3**, (1), pp. 1–11
21 Zappala, D., Tavner, P., Crabtree, C., Sheng, S.: 'Sideband algorithm for automatic wind turbine gearbox fault detection and diagnosis'. Proc. EWEA, Vienna, February 2013, pp. 1–10

## 9 Appendix: DFIG parameters

Ratings: $P_s = 30$ kW, $f = 50$ Hz and $V_s = 230$ V
Pole pairs: $p = 2$
Stator–rotor turns ratio: $n_{sr} = 1.272$
Stator and rotor resistances: $R_s = 0.079$ and $R_r = 0.044\ \Omega$
Stator and rotor self-inductances: $L_s = 0.031$ mH and $L_r = 0.019$ mH
Magnetising inductance: $L_m = 0.031$mH
Stator voltage: $V_s = 78$ V
DC-link voltage: $V_{DC} = 48$ V